Received: 23 May 2017 | Accepted: 15 June 2017

DOI: 10.1111/ijac.12743

ORIGINAL ARTICLE

International Journal of Applied Ceramic TECHNOLOGY

Photoluminescence characterization and heat treatment effect on luminescence behavior of $BaTa_2O_6:Dy^{3+}$ phosphor

Mustafa İlhan[1] | **Mete Kaan Ekmekçi**[2] | **Ayhan Mergen**[1] | **Cemalettin Yaman**[3]

[1]Department of Metallurgical and Materials Engineering, Marmara University, İstanbul, Turkey

[2]Department of Chemistry, Marmara University, İstanbul, Turkey

[3]Department of Metallurgical and Materials Engineering, Yıldız Technical University, İstanbul, Turkey

Correspondence
Mustafa İlhan
Email: mustafa.ilhan@marmara.edu.tr

Abstract

Undoped and Dy^{3+}-doped barium tantalate phosphors were synthesized by the solid-state reaction method at 1425°C. Also, 10 mol% Dy^{3+}-doped $BaTa_2O_6$ was sintered between 1150 and 1425°C in order to determine temperature effect on structural and luminescence properties. Afterwards, they were characterized by XRD, SEM-EDS and photoluminescence (PL) analyses. PL spectra exhibited the excitation peaks between 300 and 440 nm. Two typical emissions were observed at 486.2 nm (blue) and 577.7 nm (yellow) due to the $^4F_{9/2}\rightarrow{}^6H_{15/2}$ and $^4F_{9/2}\rightarrow{}^6H_{13/2}$ transitions, respectively. Emission intensities increased with increasing doping concentration of Dy^{3+} up to 10 mol% and then decreased due to the concentration quenching effect. Moreover, depending on the increase in heat treatment temperature, the intensity of emission reached maximum at 1425°C. The calculated CIE chromaticity coordinates of phosphors located in the white light region.

KEYWORDS

luminescence, scanning electron microscopy, tantalum/tantalum compounds, X-ray methods

1 | INTRODUCTION

Increasing demand of functional materials in daily life and technology require new investigations and developments for new materials such like in the optical area. Phosphors having useful and versatile properties can be promising candidates being part of many applications in many fields. Among the phosphor materials, rare-earth-doped phosphors with 4f-4f inner-shell transitions have some favorable properties such as energy saving, long lifetime, enhanced physical robustness, smaller size, faster switching, remarkable efficiency and kind environment properties. Therefore, most rare-earth elements are generally preferred for phosphor and laser materials production as dopants. Potential application fields of rare earth-doped phosphor materials include solar panels, field-emission displays (FEDs), scintillation, cathode-ray tubes (CRTs), vacuum fluorescent displays (VFDs) and white light-emitting diodes (W-LEDs).[1,2] White LEDs are generally considered to be the new generation light sources, which are able to replace the fluorescent lamps, because of their excellent features in terms of low energy consumption, fast response, mercury free, high efficiency, low voltage adjustability, environmental-friendly and energy-saving devices. Recently, Dy^{3+}-doped phosphors have been extensively studied as white LEDs because of their potential application. Furthermore, suitable yellow to blue (Y/B) emission intensity ratio provides a white light generation for Dy^{3+}-doped phosphor materials. Trivalent dysprosium ions (Dy^{3+}) generally possess two dominant emission bands; one of these bands are present in the blue region (470-500 nm) because of $^4F_{9/2}\rightarrow{}^6H_{15/2}$ transition while the other one exists in the yellow region (570-600 nm) due to $^4F_{9/2}\rightarrow{}^6H_{13/2}$ transition.[3-5]

Dielectric, photo-catalytic and optical properties of barium tantalate ($BaTa_2O_6$) have been carried out in recent years.[6-10] $BaTa_2O_6$ has three types of crystal structure, namely orthorhombic, hexagonal, and tetragonal which have tetragonal tungsten bronze (TTB) symmetry.[11] TTB

 © 2017 The American Ceramic Society

structure with the cylindrical rotation of a square group of four corner-sharing octahedral through 45° can be derived from an A-cationic-deficient perovskite structure (AMO_3). The TTB structure for oxide compounds having a general formula $A_2BC_2M_5O_{15}$ where A, B, and C correspond to cationic sites with 15, 12, and 9 C.N. (coordination number), respectively.[12-15] The TTB structure contains more cationic sites compared to the perovskite structure which allows the incorporation of atomic additives.[14]

In this manuscript, we investigated the synthesis and photoluminescence properties of the Dy^{3+}-doped $BaTa_2O_6$ ceramic phosphor materials. Despite several studies that have been done on the luminescence properties of different ion-doped TTB-type $BaTa_2O_6$, white light emitting properties have not been examined so far in the literature.[16,17] Also, structural and photoluminescence properties of $BaTa_2O_6$ were investigated depending on heat treatment temperature. Microstructural and photoluminescence characterizations were performed, XRD, SEM-EDS, and fluorometric analyses.

2 | MATERIALS AND METHODS

Undoped and 0.5, 2.5, 5, 10, 15, and 20 mol% Dy^{3+}-doped $BaTa_2O_6$ materials were synthesized by the solid-state process. Ta_2O_5 (99.9%, Alfa Aesar, Ward Hill, MA) and $BaCO_3$ (99.9%, Sigma-Aldrich, St. Louis, MO) were used as starting materials. Dy_2O_3 (99.9%, Alfa Aesar) was used as dopant material. $BaCO_3$ and Ta_2O_5 powders were weighted considering $BaTa_2O_6$ stoichiometry and then mixed and ground in an agate mortar in the presence of acetone for 20 minutes to obtain a homogeneous mixture. Subsequently, Dy_2O_3 dopant was added to the first mixture. The resultant powders were mixed accompanied by acetone about 10 minutes for further homogenization. After the elimination of acetone, homogenized powders were sintered at 1425°C for 20 hours in an electric furnace. Additionally, 10 mol% Dy^{3+}-doped $BaTa_2O_6$ phosphor powders were sintered between 1150 and 1425°C for 20 hours in order to investigate temperature-dependent structural and photoluminescence properties.

The sintered powders were characterized by X-ray diffractometer (XRD, Rigaku, Tokyo, Japan, D-MAX 2200) using Cu-K_α radiation between 2θ=20-60° at 2°/min and Ni filter. Morphologic properties and elemental compositions of sintered powders were analyzed by SEM (JSM-5910LV; JEOL, Tokyo, Japan) which is equipped with EDS (OXFORD Instruments, Abingdon, England, INCAx-Sight 7274; 133-eV resolution 5.9 keV). The electron microscope was operated at 20 kV accelerating voltage for both SEM and EDS analyses. Excitation and emission spectra were monitored by Scinco fluoromaster-FS/2 model fluorometer with an Xe-arc lamp (150 W). Measurements were carried out under room temperature.

3 | RESULTS AND DISCUSSION

3.1 | X-ray diffraction and SEM-EDS analyses

Figure 1 shows XRD patterns of 10 mol% Dy^{3+}-doped $BaTa_2O_6$ samples which were sintered between 1150 and 1425°C for 20 hours in order to observe the phase development, crystallization and photoluminescence behavior. From the XRD patterns, a phase transformation from low temperature polymorph (orthorhombic) (JCPDS card No.20-0146) to tetragonal polymorph of $BaTa_2O_6$ (JCPDS card No.17-0793) started to form at 1150°C. Depending on the heat treatment temperature, the orthorhombic phase disappeared at 1350°C and thereafter only the tetragonal phase formed between 1350 and 1425°C. Although the single phase structure was obtained at 1350°C, it is clear from the

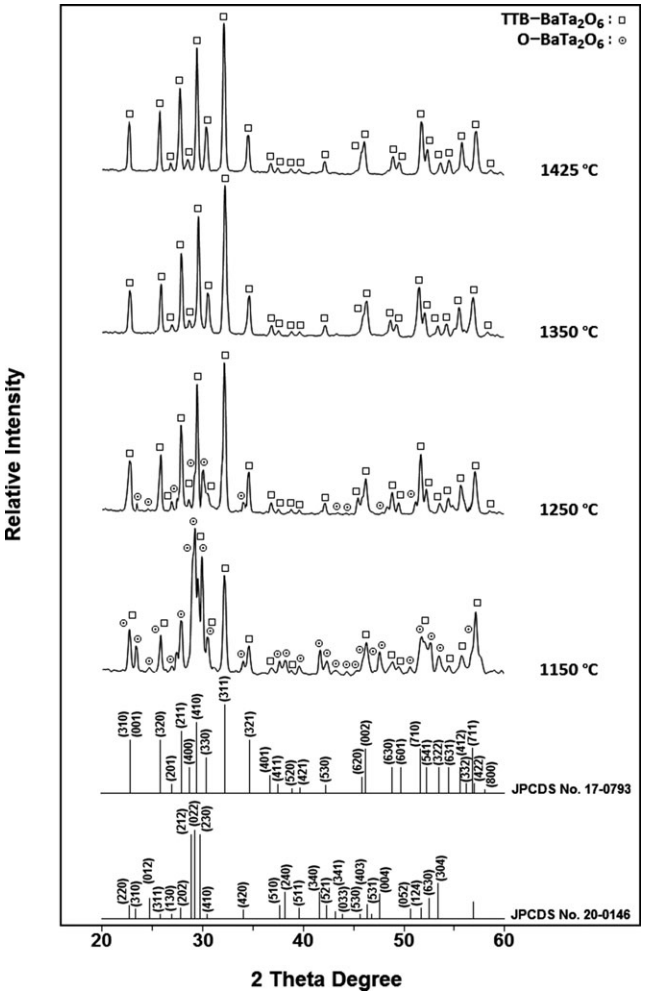

FIGURE 1 X-ray diffraction patterns for 10 mol% Dy^{3+}-doped $BaTa_2O_6$ samples sintered between 1150 and 1425°C

XRD results that the crystallization at temperature 1425°C gave the desired result. The narrowing of diffraction peaks and the flatness of background for 1425°C has clearly demonstrated this effect. Also, no any secondary phase was observed depending on the temperature change.

Figure 2 shows XRD patterns of undoped and Dy^{3+}-doped of $BaTa_2O_6$ samples between 0.5 mol% and 20 mol% which were sintered at 1425°C for 20 hours. XRD results showed that $BaTa_2O_6$ single phase (JCPDS card No.17-0793) was obtained up to 10 mol% Dy_2O_3. XRD results revealed that samples crystallized in tetragonal symmetry with space group *P4/mbm* having (no.127) TTB type structure. $BaTa_2O_6$ cell parameters have been reported as a=12.52 Å, c=3.956 Å and V=620.10 (Å)^3.[11] Also, $DyTaO_4$ secondary phase (JCPDS card No. 24-0379) was observed in 15 and 20 mol% doping concentrations.

In TTB-$BaTa_2O_6$ host structure, cation-site distribution can be predicted as; Ba^{2+} ions locate in the larger pentagonal (A) sites whereas they partially locate in the square (B) sites, while small triangular (C) sites remain empty. Based on the ion's radius and valence, the square (B) sites of TTB-$BaTa_2O_6$ structure may be occupied by smaller Dy^{3+} ions which have an ionic radius of 1.083 Å (for 9 C.N.) compared to 1.61 Å (12 C.N.) for Ba^{2+}. Also, dysprosium cations might enter into the larger pentagonal (A) sites which are available for Ba^{2+} cations. But, the vacant triangular (C) sites are too small for such occupation. The left side broadening of XRD patterns indicated a distortion due to occupation of free space sites by RE^{3+} cations in the TTB structure for doping levels up to 10 mol%. The pentagonal and square sites have a bigger lattice constant that is convenient for dopants.[16] Trivalent Dy ions which replaced Ba^{2+} ions might occupy most probably the pentagonal sites with C.N. of 15 when compared to square sites with C.N. of 12.[16,17] The schematic illustration of TTB-$BaTa_2O_6$ structure is given in Figure 3. Although $BaTa_2O_6$ single phase has maintained up to 10 mol%, the insertion of Dy^{3+} ions will have an effect on the charge compensation in the structure. Consequently, the charge compensation of TTB structure up to 10 mol% might have been compensated due to the evaporation of Ba^{2+} cations.[16-18] Over 10 mol% concentration, the incorporation of Dy^{3+} ions caused a change in the single-phase structure of $BaTa_2O_6$. Although some of the Dy^{3+} ions filled the square sites or pentagonal sites, the remaining Dy^{3+} ions promoted the formation of the $DyTaO_4$ phase. Accordingly, the change in lattice distortion decreased with increasing doping concentrations above 10 mol% due to the presence of the $DyTaO_4$ phase.

The effect of heat treatment temperature on the grain growth and phase development were investigated by SEM.

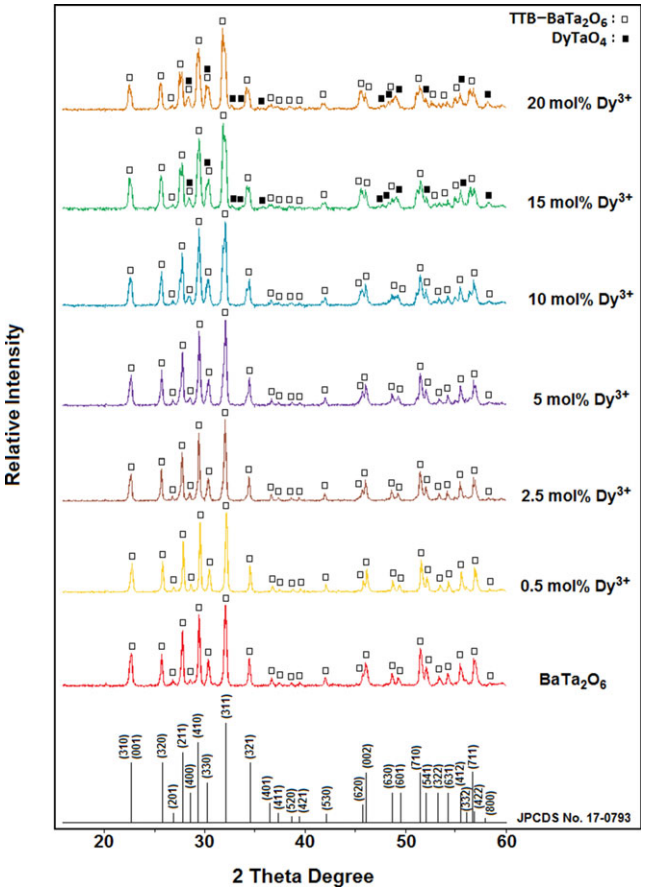

FIGURE 2 X-ray diffraction patterns for undoped and Dy^{3+}-doped $BaTa_2O_6$ between 0.5 and 20 mol% sintered at 1425°C for 20 h

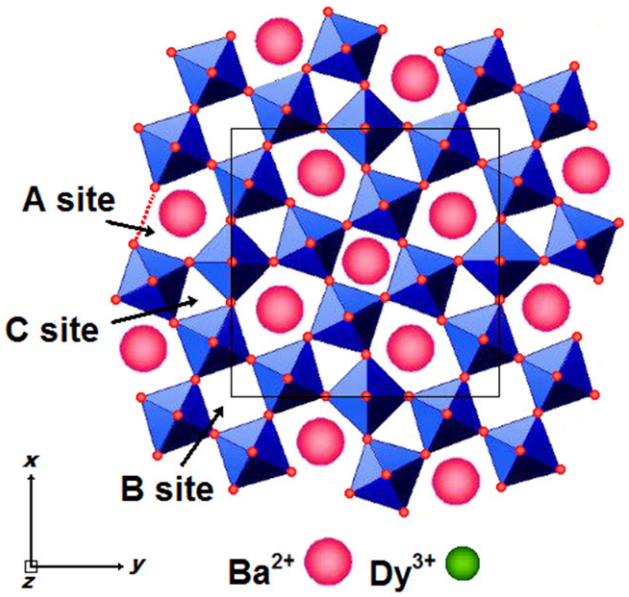

FIGURE 3 Schematic illustration for TTB-$BaTa_2O_6$ structure in the direction of z axis

Figure 4A-D gives the SEM micrographs of 10 mol% Dy^{3+}-doped $BaTa_2O_6$ powders which were sintered between 1150 and 1425°C. From the SEM observations, small grains formed at 1150°C were transformed into large grains due to heat treatment effect of 1425°C. Depending on the increase in temperature from 1150 to 1425°C, the grain size increased from 0.2-0.5 μm to 0.8-2.5 μm, respectively. Grain size growth can be interpretable by a phase transformation from orthorhombic to tetragonal between 1150°C and 1350°C.[18,19] SEM examination also showed that heat treatment has no effect on the grain shape. As seen from SEM micrographs, oval-roundish grain shape continued at all the sintering temperatures.

Figure 5A-F gives the SEM micrographs of undoped and doped powders for 0.5, 2.5, 5, 10, 15, and 20 mol% Dy^{3+} concentrations. Depending on the increase in Dy^{3+}-doping concentration, the grain size decreased and changed between 0.5 and 5 μm. The decrease in grain size could be attributed to the suppression of abnormal grain growth as a result of lattice distortion.[16,17] From SEM analysis, it was observed that the large and oval-shaped $BaTa_2O_6$ grains transformed into small and cornered shapes. Phase determination and elemental composition have been carried out by SEM-EDS analysis. EDS spectra and SEM micrographs of 15 mol% doped sample were given in Figure 6A-D and C-D, respectively. EDS analysis revealed that the elemental compositions of Dy^{3+}-doped $BaTa_2O_6$ grains (point 1) and $DyTaO_4$ large grains (point 2) were in agreement with the XRD results and theoretical composition.

3.2 | Photoluminescence analysis

The charge transfer band (CTB) of $BaTa_2O_6$ host monitored at 615.7 nm. The CTB centered at 260 has been attributed to the O^{2-}-RE^{3+} charge transfer (CT) transitions by the electron transfer from filled 2p orbital of O^{2-} ions to vacant 4f orbital of RE^{3+} ions.[17] On the other hand, the Ta–O vibrations occur at lower frequencies than Nb–O vibrations and these lower frequency contributions to the phonon density of states will give a more negative

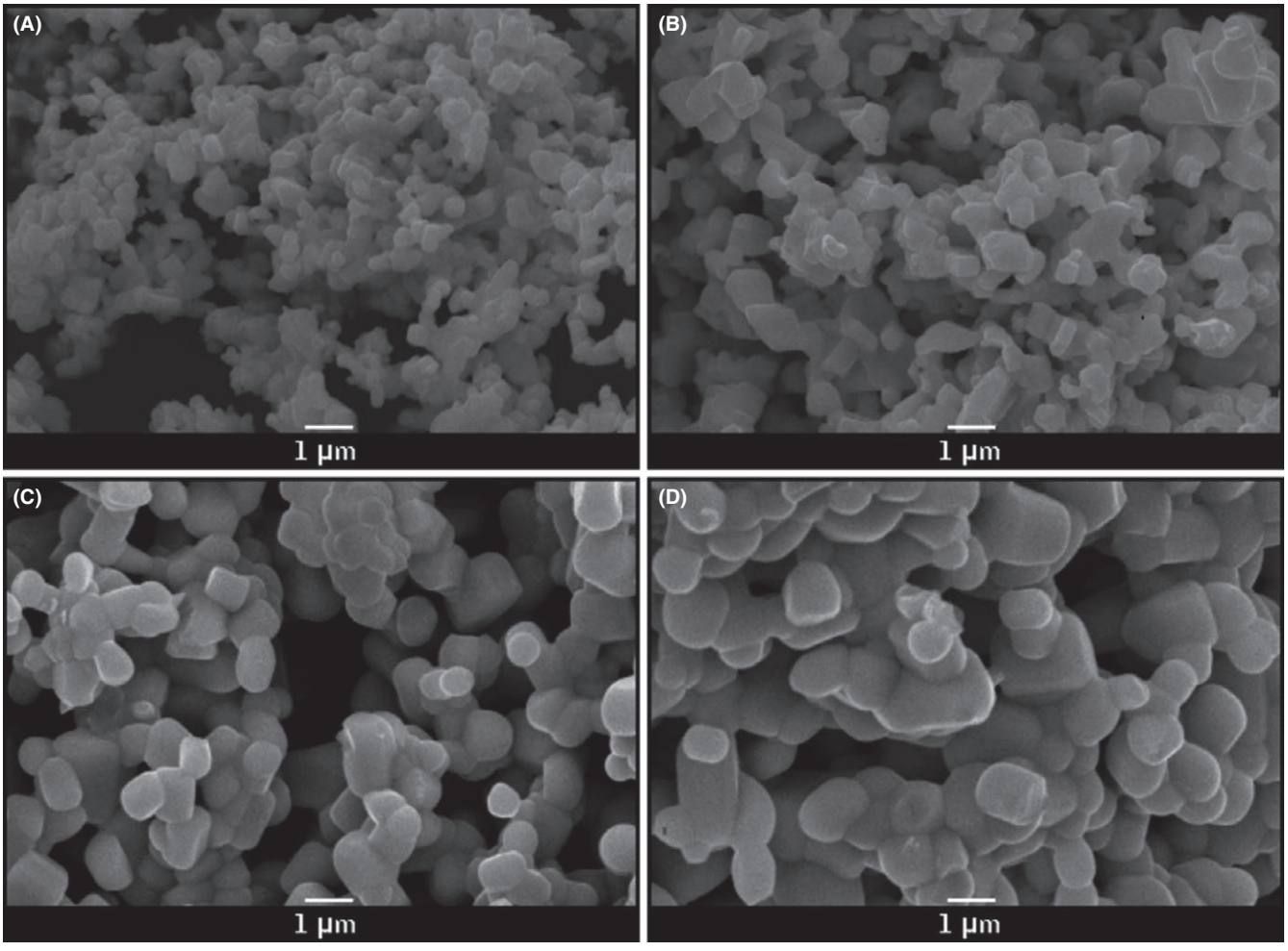

FIGURE 4 SEM micrographs of 10 mol% Dy^{3+}-doped $BaTa_2O_6$ phosphors sintered at (A) 1150°C, (B) 1250°C, (C) 1350°C and (D) 1425°C at 10 000× magnification

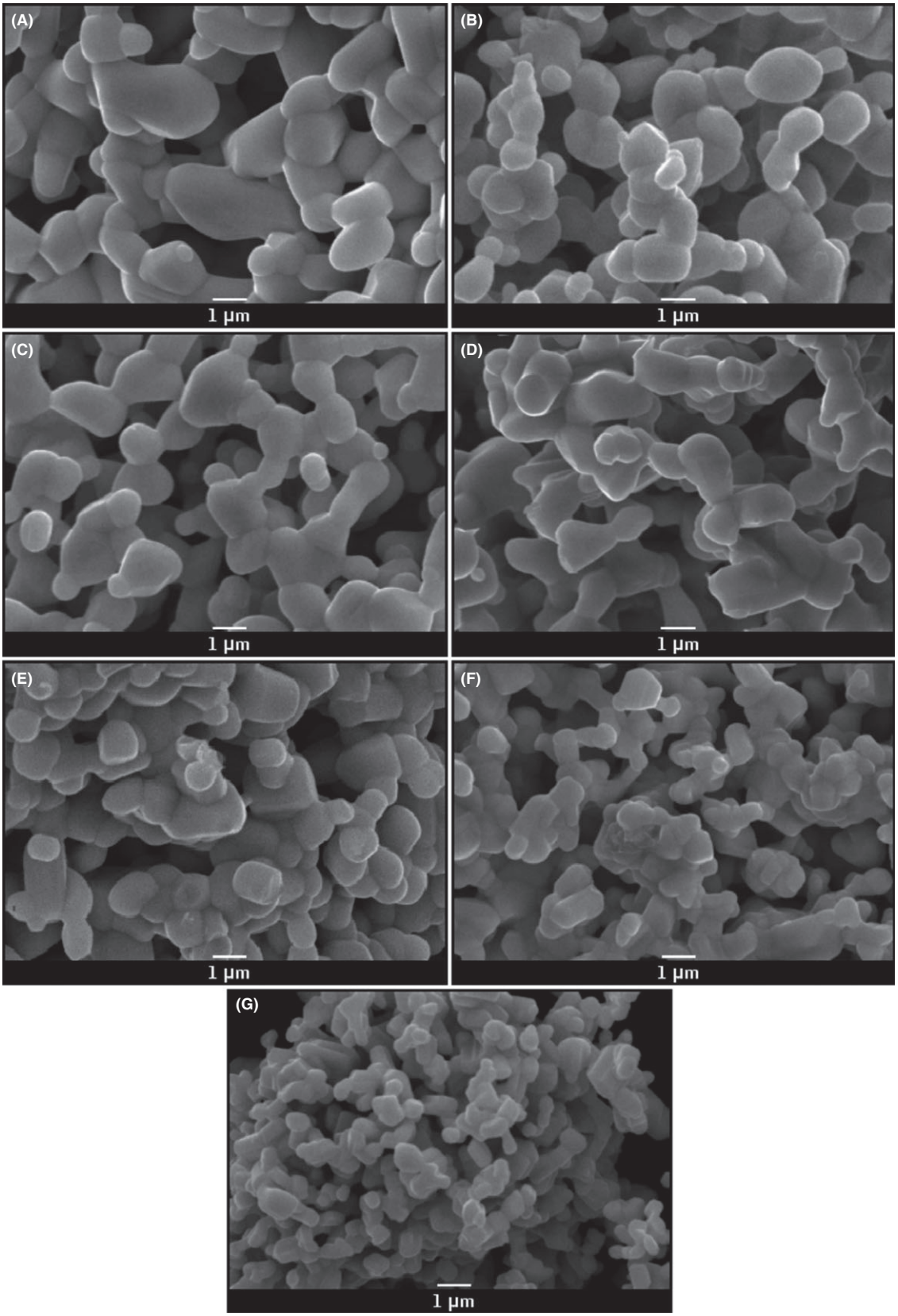

FIGURE 5 SEM micrographs of (A) undoped, (B) 0.5, (C) 2.5, (D) 5, (E) 10, (F) 15 and (G) 20 mol% Dy^{3+}-doped $BaTa_2O_6$ phosphors at 10 000× magnification

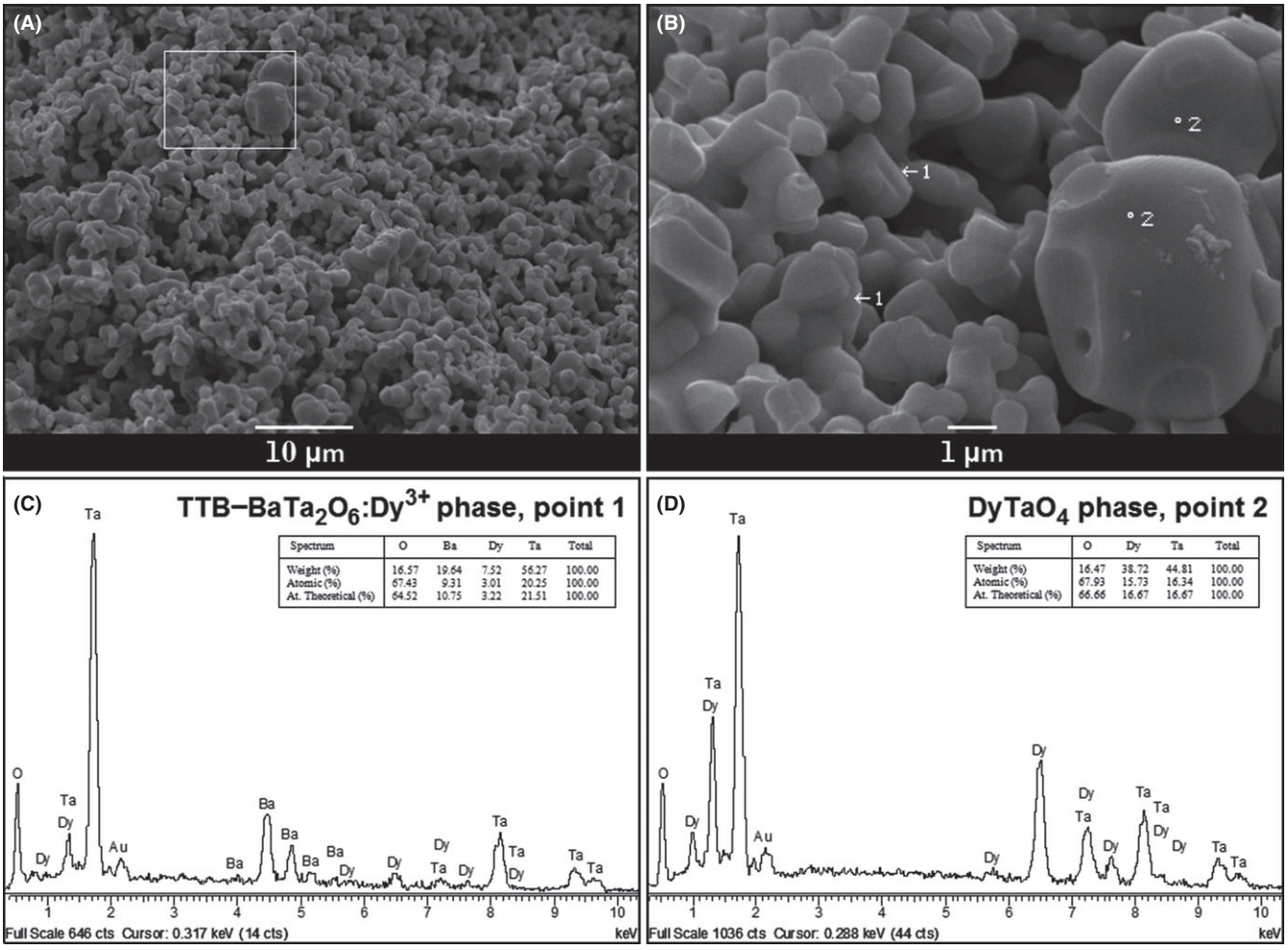

FIGURE 6 SEM-EDS results of 15 mol% Dy^{3+}-doped sample under 20 kV accelerating voltage; SEM micrographs (A) low (2000×) and (B) high (10 000×) at magnifications, EDS spectra (C) TTB-$BaTa_2O_6$:Dy^{3+} phase (point 1), (D) $DyTaO_4$ phase (point 2)

vibrational free energy for the tantalates compared with the niobates.[20] Low phonon interactions of tantalates are possibly induced by weak interactions among TaO_6 octahedrals. This will promote more excitation energy transfer to RE^{3+} ion centers within the host lattice.

Figure 7 shows the excitation spectra of $BaTa_2O_6$:xDy^{3+} ($0.5 \leq x \leq 20$ mol%) phosphors monitored under 486.2 nm emission wavelength. Five excitation bands were identified as $^6H_{15/2} \rightarrow {}^4K_{15/2}$ (326.5 nm), $^6H_{15/2} \rightarrow {}^4I_{9/2}$ (338.4 nm), $^6H_{15/2} \rightarrow {}^6P_{7/2}$ (352.4 nm), $^6H_{15/2} \rightarrow {}^4I_{11/2}$ (366.5 nm) and $^6H_{15/2} \rightarrow {}^4I_{13/2}$ (390.4 nm), as to Dieke's diagram. The emission spectra of $BaTa_2O_6$:xDy^{3+} ($0.5 \leq x \leq 20$ mol%) phosphors under 366.5 nm excitation were given in Figure 8. The $BaTa_2O_6$:Dy^{3+} phosphors exhibited two emission bands at 486.2 nm (blue region) and 577.7 nm (yellow region). Blue and yellow regions are the characteristic emissions of Dy^{3+} attributed to the $^4F_{9/2} \rightarrow {}^6H_{15/2}$ and $^4F_{9/2} \rightarrow {}^6H_{13/2}$ transitions, respectively.

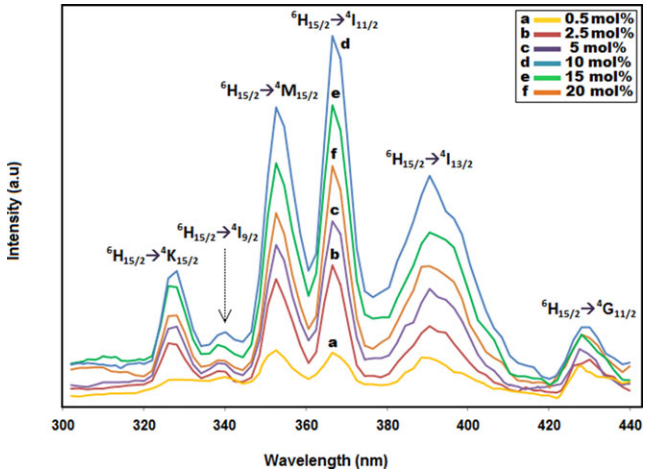

FIGURE 7 Excitation spectra of $BaTa_2O_6$:Dy^{3+} phosphors monitored at λ_{em}=486.2 nm

The luminescence intensity increased by increasing of Dy^{3+} concentration, up to 10 mol% and then decreased due to concentration quenching effect. Generally, the concentration quenching of the luminescence from a RE^{3+} ion is due to the energy transfer among the RE^{3+} activators at the high dopant concentrations. During the energy

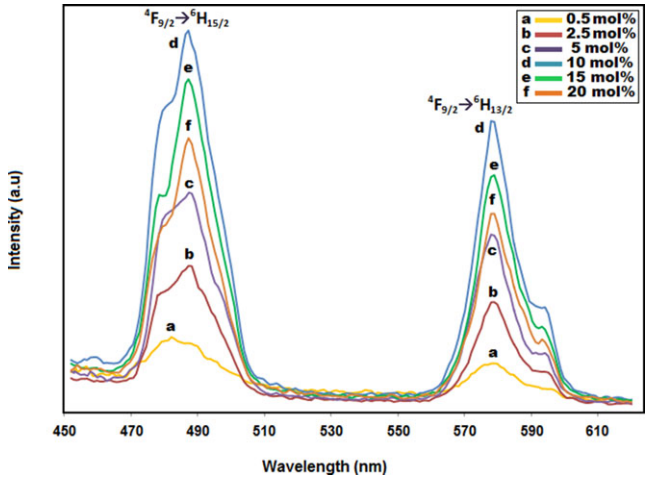

FIGURE 8 Emission spectra of $BaTa_2O_6:Dy^{3+}$ phosphors excited at λ_{ex}=366.5 nm

transfer process, the excitation energy will perish in a killer center or at a quenching site, resulting in luminescence quenching.[21] Increase in the Dy^{3+} concentration decreases the Dy^{3+}–Dy^{3+} distance which promotes nonradiative energy transfer between Dy^{3+} ions. Therefore, the possibility of nonradiative energy transfers between ions can occur at the higher concentrations. Additionally, the efficient emission can be observed only for low dopant concentration. Even for the host where the distance between dopants is relatively long as in the case phosphates where the luminescence decay profiles is strongly exponential for low dopant ($0<x\leq1$) concentrations. At greater concentrations, the decay curves become nonexponential, and the nonexponential change is prominent while the doping increases.[22,23] This shows that there is more than one relaxation mechanism as a result of concentration quenching. Blasse's equation could be used to predict the critical distance for energy transfer (R_c) in $BaTa_2O_6:Dy^{3+}$ (1):[24]

$$R_c \approx 2\left(\frac{3V}{4\pi X_c N}\right)^{1/3} \quad (1)$$

where the (V) is volume, (N) is the unit cell and (X_c) the critical concentration of dopant. For the $BaTa_2O_6:Dy^{3+}$ phosphor, X_c=0.10, V=620.10 (Å)^3 and N=2. The R_c of Dy^{3+} in $BaTa_2O_6:Dy^{3+}$ was calculated as 18.09 Å. The nonradiative energy transfer and the luminescence of oxidic phosphors are based on resonance energy transfer by electric multipole–multipole interaction or exchange interaction.[25] This case might be attributed to Blasse's theory,[26] just a multipole–multipole interaction occurs when the critical distance is >5 Å, the exchange interaction becomes noneffective. When the critical distance is shorter than 5 Å, the exchange interaction becomes effective. Because, the R_c value was calculated as 18.09 Å, the effective mechanism of concentration quenching for $BaTa_2O_6:Dy^{3+}$ phosphor was found to be multipolar interaction. An explanation is required in order to determine multipolar interaction. It was reported by Van Uitert,[27] the strength or type of the multipolar interaction can be determined from this equation (2):

$$I/x = K\left[1+\beta(x)^{\theta/3}\right]^{-1} \quad (2)$$

The (x) indicates the dopant concentration which should not be less than the critical concentration. The (I/x) is the emission intensity, while (K) and (β) are constants for a $BaTa_2O_6:Dy^{3+}$ crystal. The (θ) value indicates the electric multipolar type; where θ=3 for the energy transfer among the nearest-neighbor ions (exchange interaction), while θ=6 for dipole-dipole (d-d), θ=8 dipole-quadrupole (d-p) and θ=10 quadrupole-quadrupole (q–q) interactions. Assuming that $\beta(x)^{\theta/3} \gg 1$, equation (2) can be simplified as follows:

$$log(I/x) = K' - \theta/3 logx (K' = logK - log\beta) \quad (3)$$

The electric multipolar type (θ) can be calculated from the slope of equation (3) taking in the consideration that slope ($-\theta/3$) of the plot log(I/x) and log(x). The critical concentration is 10 mol% which is the start value for concentration quenching. Slope was calculated by taking values from critical concentration to highest concentration. The plot of log(I/x) as a function of log(x) in $BaTa_2O_6:Dy^{3+}$ phosphors are indicated in Figure 9. According to this plot, it is clear that the relevance of log(I/x) on log(x) of Dy^{3+} is

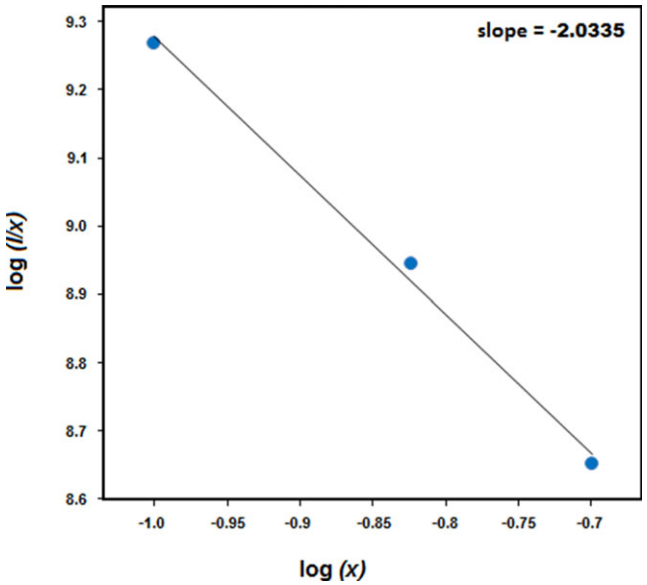

FIGURE 9 Relation between the log_{10}(I/x) and log_{10}(x) of Dy^{3+} for $BaTa_2O_6:Dy^{3+}$ phosphors

linear and the calculated value of its slope is about −2.0335. Then, the value of θ can be calculated as nearly 6. This θ value demonstrates that energy transfer mechanism for $BaTa_2O_6$:Dy^{3+} phosphor is the dipole-dipole (d-d) interaction.

Figure 10 shows the dependence of blue (B) and yellow (Y) emission spectra of $BaTa_2O_6$:xDy^{3+} ($0.5 \leq x \leq 20$ mol%) phosphors excited under 366.5 nm. It is well known that the $^4F_{9/2} \rightarrow {}^6H_{15/2}$ transition is blue in color and has a magnetic dipole transition that hardly changes the crystal field strength around the Dy^{3+} ions. In addition, the Dy^{3+} ions have a high symmetry in this transition when located in the host. Despite the fact that the local ion symmetry does not affect the magnetic dipole transition intensity, the symmetry has a strong influence on the number of Stark levels observed in the spectra.[22] However, the $^4F_{9/2} \rightarrow {}^6H_{13/2}$ transition is yellow color and has an electric dipole transition which can be affected strongly by the local environment of the active ion. Therefore, high symmetry crystal sites are not allowed. The Dy^{3+} ions are very susceptible to the crystal field changes due to their low symmetry. The emission intensity ratio yellow/blue (Y/B) of electric dipole to magnetic dipole has been used to explain the symmetry of the local environment of the RE^{3+} ions.[28] As seen in Table 1 and Figure 10, the low Y/B ratio (between 0.67 and 0.84) for the $BaTa_2O_6$:Dy^{3+} phosphors indicated a lower degree of covalency or interaction between dysprosium and oxygen ions. The reason for this might beong the evaporation of Ba^{2+} from pentagonal and square sites in the TTB lattice which led to no change in the covalency.

Figure 11 shows the emission spectra of 10 mol% Dy^{3+} -doped $BaTa_2O_6$ phosphors excited under 366.5 nm

TABLE 1 CIE color coordinates, CCT data, and Y/B ratios of $BaTa_2O_6$ phosphors at different Dy^{3+} concentrations and excited at λ_{ex}=366.5 nm

		CIE coordinates		
Dy^{3+} concentration (%)	Y/B	*x*	*y*	CCT
0.5	0.67	0.258	0.331	9980
2.5	0.72	0.265	0.332	9437
5	0.84	0.281	0.344	8105
10	0.76	0.275	0.337	8622
15	0.70	0.262	0.331	9686
20	0.72	0.264	0.332	9508

that synthesized at 1150 (A), 1250 (B), 1350 (C) and 1425°C (D), respectively. Depending on the increase in temperature from 1150 to 1425°C, the emission intensities of $^4F_{9/2} \rightarrow {}^6H_{15/2}$ and $^4F_{9/2} \rightarrow {}^6H_{13/2}$ transitions increased due to phase development and improved crystallinity as mentioned before. Also, as seen from the Figure 11, increasing the yellow/blue ratio indicated the structure with high symmetry which depends on the increase in temperature. Hence, the best emission intensity was observed for sample D which was heat treated at 1425°C. In addition, colored pictures of 10 mol% Dy^{3+} -doped $BaTa_2O_6$ phosphors were taken under 366 nm UV-light excitation,using CAMAG Model UV lamp in a dark room. As seen from the colored pictures, enhanced crystallinity obtained for 10 mol% Dy^{3+} -doped $BaTa_2O_6$ phosphor at 1425°C has led to bright greenish-yellow emission, while the others have a weak luminescence.

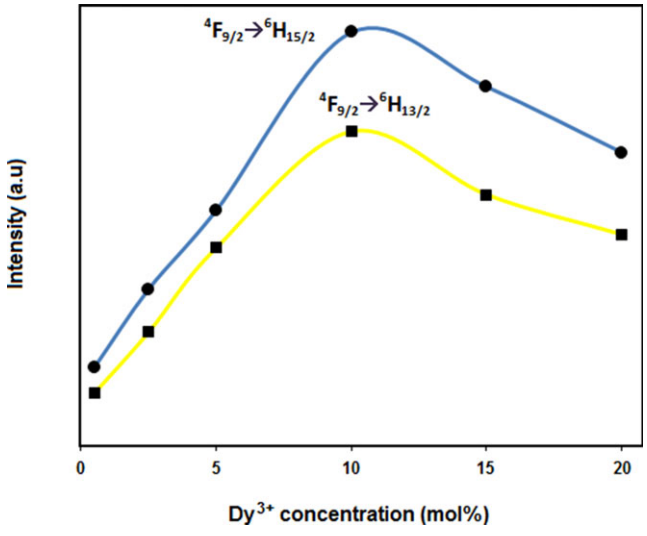

FIGURE 10 Dy^{3+} concentration dependence of magnetic dipole and electric dipole emission intensities for $BaTa_2O_6$:Dy^{3+} phosphors

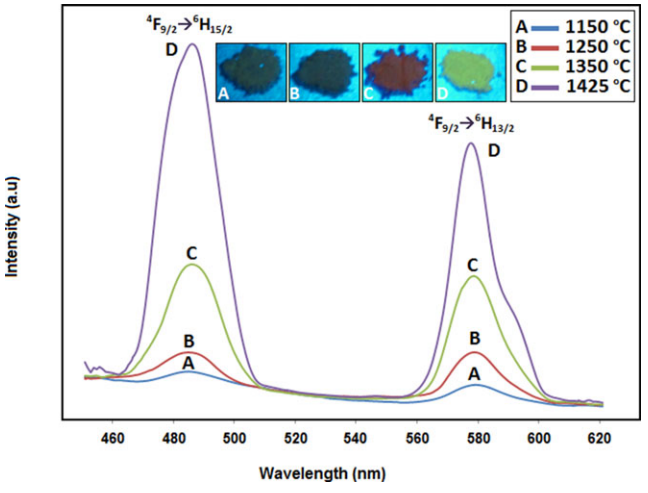

FIGURE 11 Emission spectra of 10 mol% Dy^{3+}-doped $BaTa_2O_6$ phosphors sintered between 1150 and 1425°C at λ_{ex}=366.5 nm. Colored pictures of 10 mol% Dy^{3+}-doped $BaTa_2O_6$ phosphors taken under 366 nm UV light excitation

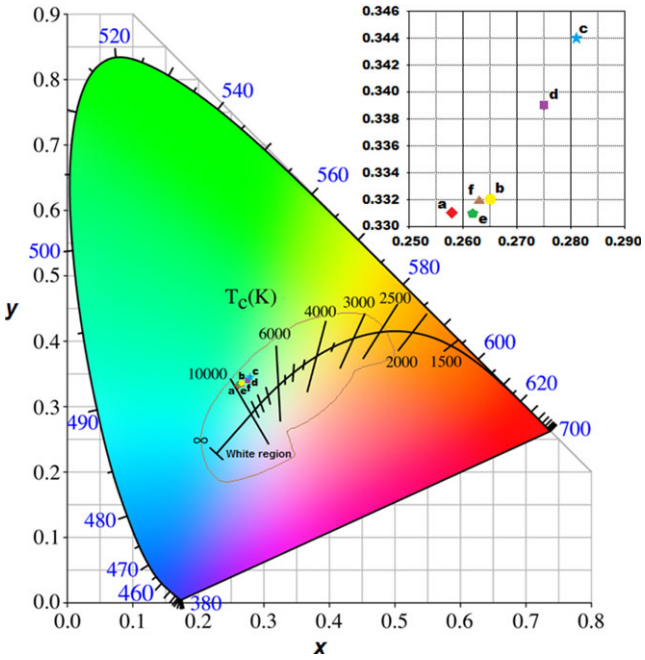

FIGURE 12 The Commission Internationale de I'Eclairage CIE coordinates of $BaTa_2O_6$:xDy^{3+} (x=a:0.5, b:2.5, c:5, d:1.0, e:15 and f:20 mol%) phosphors excited at 366.5 nm

The chromaticity coordinates (*x*,*y*) of $BaTa_2O_6$:Dy^{3+} phosphors with different doping concentrations excitation under 366.5 nm were listed in Table 1 which were declared by The Commission Internationale de I'Eclairage (CIE). The chromaticity coordinates were determined from the PL spectra of different concentration Dy^{3+}-doped $BaTa_2O_6$ phosphor and the corresponding CIE chromaticity diagram was presented in Figure 12. As seen from all concentrations of $BaTa_2O_6$:Dy^{3+} phosphors, the obtained values indicated (greenish-blue) the white region. The light quality of a source is evaluated through the correlated color temperature (CCT) values which demonstrates the temperature of the closest Plankian black-body radiator to the operating point on the chromaticity diagram. The CCT values were calculated, using the McCamy empirical formula (4) and was expressed as where $n=(x-x_e)/(y-y_e)$ is the inverse slope line, and x_e=0.332 and y_e=0.186.[29]

$$CCT = -449n^3 + 3525n^2 - 6823n + 5520.33 \quad (4)$$

The CCT values at different concentrations are presented in Table 1. The CCT values for the $BaTa_2O_6$:Dy^{3+} phosphors changed in the range of 8105-9980 K. It was found that the CCT value for 10 mol% was 8622 K. Moreover, the greenish-yellow colored picture of the 10 mol% sample at 1425°C is in Figure 11 , which confirmed the location of color coordinates for 10 mol% in the CIE diagram. As seen in Table 1, the CCT values of all the phosphors were found to be higher than that of the standard white light luminescence. In the literature, the reported CCT source values mostly range from 3500 to 6500 K. However, recently high intensity and ultra-high intensity white light emitting diodes have been introduced as light sources for optical microscopy, and have color temperatures ranging from 6.500 to 9.500 K, rivaling daylight. This study indicates that the Dy^{3+}-doped barium tantalate phosphor is expected to be a promising candidate for white-emitting phosphor for near-ultraviolet (NUV) white light-emitting diodes.

4 | CONCLUSIONS

Undoped and Dy^{3+}-doped TTB-$BaTa_2O_6$ phosphors were produced by the conventional solid-state method. Also, 10 mol% Dy^{3+}-doped $BaTa_2O_6$ was synthesized between 1150 and 1425°C in order to determine the temperature effect on structural and photoluminescence properties. Depending on the heat treatment temperature, orthorhombic phase has disappeared at 1350°C and the tetragonal phase has formed between 1350 and 1425°C. From the SEM results, grains are small sized at 1150°C, while they became larger due heat treatment at 1425°C. SEM analysis also showed that $BaTa_2O_6$:Dy^{3+} grain size decreased with the increasing Dy^{3+} concentration. Increase in temperature from 1150 to 1425°C led to an increase in the emission intensities due to phase development and improved crystallinity. $BaTa_2O_6$:Dy^{3+} phosphors exhibited $^4F_{9/2}\rightarrow{}^6H_{15/2}$ at 486.2 nm (blue) and $^4F_{9/2}\rightarrow{}^6H_{15/2}$ at 577.7 nm (yellow) transitions. The emission intensity increased up to 10 mol% concentration and then decreased due to concentration quenching effect. Depending on the increase in temperature, the emission intensities of $^4F_{9/2}\rightarrow{}^6H_{15/2}$ and $^4F_{9/2}\rightarrow{}^6H_{13/2}$ transitions increased due to phase transformation and improved crystallinity. The CIE chromaticity coordinates for all $BaTa_2O_6$:Dy^{3+} phosphors located in the white region. The present results imply that the $BaTa_2O_6$:Dy^{3+} phosphor material could have a potential for white LEDs in NUV applications.

REFERENCES

1. Marciniak L, Stefanski M, Tomala R, Hreniak D, Strek W. Synthesis and spectroscopic properties of $RbLa_{1-x}Eu_xP_4O_{12}$ nanocrystals. *J Alloy Compd*. 2015;624:210-215.
2. Erdem M, Ekmekci MK, Orucu H, Bilir G. Structural and spectroscopic properties of d-$Y_2Si_2O_7$ nanopowders activated with Nd^{3+} ions. *Int J Appl Ceram Technol*. 2015;12:1016-1019.
3. Nakamura S, Fasol G. *The Blue Laser Diode: Gan Based Light Emitters and Laser*. Berlin, Germany: Springer; 1997.
4. Levine AK, Palilla FC. A new, highly efficientred-emitting cathodeluminescent phosphor (YVO_4:Eu) for color television. *Appl Phys Lett*. 1964;5:5118-5120.

5. İlhan M, Ekmekçi MK. Synthesis and photoluminescence properties of Dy^{3+} doped white light emitting $CdTa_2O_6$ phosphors. *J Solid State Chem*. 2015;226:243-249.
6. Layden GK. Dielectric and structure studies of hexagonal $BaTa_2O_6$. *Mater Res Bull*. 1968;3:349.
7. Kovba LM, Lykova LN, Paromova MV, Lopato LM. Barium oxide-tantalum oxide system. *Russ J Inorg Chem*. 1977;22:1544.
8. Ichinose N, Shimada T. Effect of grain size and secondary phase on microwave dielectric properties of $Ba(Mg_{1/3}Ta_{2/3})O_3$ and Ba $([Mg, Zn]_{1/3}Ta_{2/3})O_3$ systems. *J Eur Ceram Soc*. 2006;26:1755-1759.
9. Lee YH, Kim YS, Kim DH, Oh MH. Conduction mechanisms in barium tantalates films and modification of interfacial barrier height. *IEEE T Electron Dev*. 2000;47:71-76.
10. Kato H, Kudo A. New tantalate photocatalysts for water decomposition into H_2 and O_2. *Chem Phys Lett*. 1998;295:487-492.
11. Layden GK. Polymorphism of $BaTa_2O_6$. *Mater Res Bull*. 1967;2:533-539.
12. Magneli A. The crystal structure of tetragonal potassium tungsten bronze. *Ark Kemi*. 1949;1:213-221.
13. Hyde BG, O'Keefe M. Relations between the $DO_9(ReO_3)$ structure type and some `bronze' and `tunnel' structures. *Acta Crystallogr A*. 1973;29:243-248.
14. Roulland F, Josse M, Castel E. Influence of ceramic process and Eu content on the composite multiferroic properties of the $Ba_{6-2x}Ln_{2x}Fe_{1+x}Nb_{9-x}O_{30}$ TTB system. *Solid State Sci*. 2009;11:1709-1716.
15. Tressaud A. Structural architecture and physical properties of some inorganic fluoride series: a review. *J Fluorine Chem*. 2011;132:651-659.
16. İlhan M. Synthesis, structure and photoluminescence properties of Ho^{3+} doped TTB– $BaTa_2O_6$. *Solid State Sci*. 2014;38:160-168.
17. İlhan M, Ekmekçi MK, Mergen A, Yaman C. Synthesis and optical characterization of red-emitting $BaTa_2O_6$:Eu^{3+} phosphors. *J Fluoresc*. 2016;26:1671-1678.
18. İlhan M, Mergen A, Yaman C. Removal of iron from $BaTa_2O_6$ ceramic powder produced by high energy milling. *Ceram Int*. 2013;39:5741-5750.
19. Zeng P, Wang K, Falkenstein-Smith RL, Ahn J. Effects of sintering temperature on the performance of $SrSc_{0.1}Co_{0.9}O_{3-\delta}$ oxygen semipermeable membrane. *Braz J Chem Eng*. 2015;32:757-765.
20. Mumme WG, Grey IE, Roth RS, Vanderah TA. Contrasting oxide crystal chemistry of Nb and Ta: the structures of the hexagonal bronzes $BaTa_2O_6$ and $Ba_{0.93}Nb_{2.03}O_6$. *J Solid State Chem*. 2007;180:2429-2436.
21. Zhang W, Seo HJ. Luminescence and structure of a novel red-emitting phosphor Eu^{3+}-doped tellurate garnet $Li_3Y_3Te_2O_{12}$. *J Alloy Compd*. 2013;553:183-187.
22. Marciniak L, Hreniak D, Strek W. Controlling luminescence colour through concentration of Dy^{3+} ions in $LiLa_{1-x}Dy_xP_4O_{12}$ nanocrystals. *J Mater Chem C*. 2014;2:5704-5708.
23. Chemingui S, Ferhi M, Naifer KH, Férid M. Synthesis and luminescence characteristics of Dy^{3+} doped $KLa(PO_3)_4$. *J Lumin*. 2015;166:82-87.
24. Blasse G. Energy transfer between inequivalent Eu^{2+} ions. *J Solid State Chem*. 1986;62:207-211.
25. Blasse G, Grabmarier BC. *Luminescent Materials*. Berlin: Springer-Verlag; 1994:99.
26. Blasse G. Energy transfer in oxidic phosphors. *Philips Res Rep*. 1969;24:131.
27. Van Uitert LG. Characterization of energy transfer interactions between rare earth ions. *J Electrochem Soc*. 1967;114:1048-1053.
28. Vijaya N, Kumar KU, Jayasankar CK. $Dy^{(3+)}$-doped zinc fluorophosphate glasses for white luminescence applications. *Spectrochim Acta A*. 2013;113:145-153.
29. McCamy CS. Correlated color temperature as an explicit function of chromaticity coordinates. *Color Res Appl*. 1992;17:142-144.

How to cite this article: İlhan M, Ekmekçi MK, Mergen A, Yaman C. Photoluminescence characterization and heat treatment effect on luminescence behavior of $BaTa_2O_6$:Dy^{3+} phosphor. *Int J Appl Ceram Technol*. 2017;00:1-10. https://doi.org/10.1111/ijac.12743